United States Department of the Interior

Geological Survey

Multichannel Seismic Measurements

On the Northern Edge of

the Bahaman-Cuban Collision Zone

Mahlon M. Ball, Editor

Open-File Report 83-23

This report is preliminary and has not been reviewed for
conformity with U.S. Geological Survey editorial standards.

Table of Contents   Page

Introduction

Mahlon M. Ball, Ray G. Martin, Richard Sylwester, and Wayne D. Bock

General

This paper presents geophysical data obtained in the western reaches of the Old Bahama Channel separating Cuba and the Bahamas (Figure 1). These data were collected as part of an ongoing investigation of Caribbean and Bahaman geology primarily conducted by University of Miami and the U.S. Geological Survey (USGS). The work was done on the R/V Gilliss of Rosenstiel School of Marine and Atmospheric Sciences, (RSMAS), University of Miami. The scientific party included members of the Woods Hole Oceanographic Institute (WHOI) and RSMAS.

Previous Work

Geology in Cuba is complicated. Meyerhoff and Hatten (1968) clearly illustrate this complexity in their paper on salt diapirs in central Cuba in which they present a good and admirably referenced summary of the islands' geologic history. From their synthesis, it appears that Cuba is composed of a melange of largely Mesozoic rocks with the oldest, igneous and metamorphic rocks on the south, bordered by volcaniclastics, containing some displaced serpentinites and gabbroic complexes, that in turn are flanked by predominantly carbonate rocks and evaporites on the north (Figure 2). The serpentinites although rooted in the south are concentrated by flowage along a median welt that runs the length of the island and roughly separates the volcaniclastics on the south from the carbonates and evaporites. The welt is the locus of a regional gravity minimum. All rocks have been pushed, folded and thrust toward the north (Figure 2). Flowage of serpentinites along major thrust fault planes is inferred. Flowage of salt on thrusts in the northern

1

carbonate province with attendant formation of diapirs is documented by rilling (Figure 3). Different rock types are commonly in fault contact with each other and intrusions are abundant.

Furrazola-Bermudez and others (1964) and Tator and Hatfield (1975 a and b) contain the lithologies and ages of sediments encountered in a number of deep wells along Cuba's north coast (Figure 1). These data are summarized and reproduced in Figure 4. Clearly, drilling has established evidence for the predominance of Jurassic and Cretaceous carbonates and evaporites in the northern coastal zone. Occurrences of repeated section in some of these wells, for example Manuy 1, indicate presence of thrusting into the area of offshore islands including Cayo Coco and Cayo Frances.

Pardo (1975) presents details of various facies and structural styles encountered in belts that strike more or less along the length of the present island. These belts are best exposed in central Cuba in eastern Matanzas, Las Villas and western Camaguey provinces. From Pardo's descriptions, the carbonates of the north coast appear to consist of shallow water platform types with evaporites in the Upper Jurassic and Lower Cretaceous. Dense cherty marls and limestones rich in pelagic organisms occur in the Albian to Coniacian section. Fragmental, conglomeratic limestones and marls comprise the Maestrichtian and early to middle Eocene strata. Toward the south in the carbonate zone, belts contain increasing amounts of dark cherty carbonates rich in pelagics and fragmental, conglomeratic limestones ranging in age from Late Jurassic to middle Eocene. Pardo (1975) points out that the carbonate facies of onshore Cuba are reminiscent of those in the present Bahamas. That is, they suggest the presence of shallow platforms separated by deep water tongues.

Mattson (1975) has assembled a set of important papers on Cuban geology

several of which had not previously been available in English. Among these papers, Rigassi (1961) is particularly noteworthy in that he emphasizes the possible role of a gigantic left-lateral strike-slip fault displacing the carbonates and evaporites of the north coast many hundreds of kilometers northwestward. Wassall (1957) adds knowledge of the range of structural styles extant on the island by describing the role of block faulting associated with uplift, subsequent to thrusting. Mattson (1973) interjects the possibility of gravity slides causing northward transport of thrust sheets seen in both Cuba and Puerto Rico. He further postulates a cessation of southward underthrusting beneath Cuba during the Eocene because the Bahaman-Cuban collision choked off the Benioff zone along Cuba's north coast. According to Mattson (1973), left-lateral strike-slip motion in the Cayman Trough south of Cuba began at this time as Cuba became part of the North American Plate.

Marine investigations have established the existance of tectonism in the Old Bahama Channel off Cuba's north coast. On the basis of single-channel measurements, Idris (1975) inferred the presence of a diapir just southeast of the southeast corner of Cay Sal Bank. This feature is shown in Figure 5. Although the shallow sub-bottom reflections are obscured by a bubble pulse, closure over an anticline at the southeast end of the profile is discernible to within the upper 0.1 second or about 100 meters below the sea floor. The apparent width of the anticline is about 1.5 km. Maximum observed structural relief appears to be somewhat less than 100 meters at 0.4 to 0.5 seconds or 500m sub-bottom. Below this depth, adjacent beds dip at barely perceptible angles toward the structureless core of the anticline. This deeper inward dip suggests the possible existence of a rim syncline and for this reason the feature is interpreted to be an evaporitic piercement structure.

Adjacent single channel records (Figure 1) also revealed three tilted blocks with apparent widths of 10 to 20 km and reliefs of at least 1 km (Figure 6). The blocks rise to within a few hundred meters of the seafloor and show some indication of internal stratification in their upper few tenths of second of reflections although they generally lack good coherent reflections. These blocks occur in a region of 5.9 km/sec refraction velocity at depths only slightly greater than 2 km (Sheridan and others, 1966) and lack any magnetic anomaly. Because of this, Idris (1975) inferred them to be cemented, shallow water carbonate platform material buried in unconsolidated sediments.

Marine single channel records are sufficient to demonstrate the interesting nature of structure along the suture between Cuba and the Bahamas. However, multiples generally obscure all but the upper 0.7 second of sub-bottom data in these profiles. The purpose of our survey was to use multichannel measurements to discover details of the deeper structure.

Our report begins with a description of the seismic system used to obtain our measurements and processing techniques used in preparing our data for presentation. Then, we present and describe our seismic sections. Finally, we discuss the implications of our data relative to geologic history of the Bahamas and Cuba and to the potential for oil and gas in this region.

Equipment

Robert M. Bowles, Mahlon M. Ball

David Taylor, and Elizabeth L. Coward

The seismic system consisted of a digital recorder with automatic gain ranging over a 500 ms window, a 12 channel hydrophone streamer with an 1100 meter long, active section and a Bolt[1] airgun energy source. Recording

sampling interval was 4 ms and lengths of records were 5 to 6 seconds when a 550 cu. in. airgun served as energy source and 3 seconds when a 40 cu. in. gun was employed. Data were recorded in SEG-Y format. The streamer contained 12 active elements 50 m long separated by 50 m passive sections to attain 100 m group intervals. The center of the streamers nearest active element was 315 m astern of the gun position. The distance from the gun to the center of the farthest active element was 1415 m. Shot points were spaced 50 m apart in order to obtain a 12 fold stack.

Navigation was supplied by a Western Geophysical Survey and Data Management System utilizing a Hewlett-Packard 2112 minicomputer and interface circuitry to integrate data from six navigation sensors. The sensors were of two types: 1) Velocity output including: range-range Loran, bottom-lock (pulsed) sonar, doppler (continuous) sonar, and gyroscope. 2) Position output including: Navy Navigation Satellite receiver and a hyperbolic loran. The navigation system triggered the seismic systems airguns at 50 meter intervals and fed velocity information to a Bell Aerospace BGM-3 gravimeter. A Lacoste-Romberg (LR) sea-going gravimeter and recording system was used for back-up and cross-checking against the Bell meter. Both the LR and Bell data were recorded on the navigation tape and the LR processed directly with post cruise analysis of the navigation information to produce track charts and gravity profiles.

In addition to CDP seismic and gravity data, total field magnetic measurements were obtained using a Varian proton magnetometer. High resolution seismic data were also recorded using a single channel streamer, analog recorder and 5 inch airgun.

Seismic Data Processing

David Taylor, Mahlon M. Ball,

Richard Sylwester, and Elizabeth L. Coward

The original time sections were generated by Phillips Petroleum Company in Bartlesville, Oklahoma. Their processing sequence was as follows:

Merge Trace Header with Demultiplexed Tapes

Apply Static Correction (for source and cable depth)

General Velocity Analysis

Detailed Velocity Search

True Amplitude Gain Control (with correction for spherical divergence)

Deconvolution

Filter (10-60) Hz

Stack (12 fold)

Filter (10-45) Hz

Deconvolution

Automatic Gain Control (with 500 ms window)

Display

The high quality of the resulting time sections indicates acquisition and processing were performed effectively.

The following is a discussion of the processing steps taken by the USGS to produce a True Relative Amplitude Section, a Scaled Section, a Migrated Section, and a Migrated Depth Section. This processing was performed on a Raytheon Data System machine and software supplied by Seismograph Service Company of Tulsa, Oklahoma. The processing steps taken up to migration and depth conversion include:

Shooting Geometry Generation

Horizontal Gain Balance

Common-Depth-Point (CDP) Sort

Pre-stacking Velocity Analysis Processing

Editing CDP Records for Analysis

500 MS Automatic Gain Control (AGC)

Mute Refracted Events

Broad-Band Filter

Predictive Deconvolution

Stacking Velocity Analysis

Pre-stack Processing

Spherical Divergence Gain Correction

Broad-Band Filter

Mute Refracted Events

Predictive Deconvolution

Normal Move-out (NMO) Correction

CDP Stack

Time Variant Band-Pass Filter

Long Period Dereverberation

The general processing flow for the above steps is shown in figure 7.
Field data quality is considered to be good with little or no editing after
playing out the field records. Standard marine geometry information inserted
into the trace headers included CDP number, trace number, and shot-to-receiver
offset distances. A trace-to-trace horizontal balance was applied on each
record to compensate for the fall-off of energy with greater shot-to-receiver
offset distances. Traces were then sorted into common-depth-point gathers.

Prior to velocity analysis, filter analysis and autocorrelation programs
were run. Editing of the CDP gathers used in velocity analysis provided 5

7

adjacent CDP's per analysis group spaced every 50 CDP's along the line. These records were then filtered using a broad band 10 to 45 Hz filter, deconvolved to attenuate short path multiples, muted to suppress first arrivals and refracted events, and scaled with a medium window AGC function. The velocity analysis program used these "clean" records to generate velocity spectra displays. The displays were used to determine the NMO correction functions which were applied at various points along the line. These functions are printed at the top of each section..

Prior to normal move-out correction and stacking of the common-depth-point gathers, a spherical divergence gain correction was applied to account for the attenuation of the data with increasing depth. Also applied were the same steps run prior to velocity analysis with the exception of the medium, window AGC scale. Normal move-out corrections were then applied and a 12 fold horizontal stack was performed to produce a raw stack section.

Filter analysis and autocorrelation programs were run on the raw stack section and a time-variant, band-pass filter was applied along with a long-period predictive deconvolution which attempted to attenuate the water-bottom multiple. Final filter and deconvolution parameters are specified in the side label on each section. This section was then put to film and labeled as the True Relative Amplitude section. A 300 ms AGC was applied to the stack section at this point and this section was also prepared for film output and labeled as the Scaled section. Finite-difference Wave Equation Migration was applied to the Scaled section and the result was prepared for film output and labeled as the Migrated section. The processing flow for migration through depth conversion is shown in figure 8.

In order to produce the migrated depth section, the original stacking velocities were smoothed laterally so as to produce the proper interval

8

velocities for the depth-conversion process. The smoothing program statistically weights the functions, and based on a laterally sliding window, assigns a new smooth function to every stacked trace on the line. The new smoothed functions were used in the depth-conversion program and applied to the migrated time section to produce the Migrated Depth section. This section was then prepared for film plotting and the depth scale drafted on the film output. Figure 9 is an iso-velocity plot of the original stacking velocities before velocity smoothing. Figure.10 is another iso-velocity plot prepared from the smoothed velocity functions. Note that the sharp differences between velocity functions in the unsmoothed velocity plot has been removed by the smoothing program. The smoothed velocity functions used in the depth-conversion program are displayed at the top of the Migrated Depth section.

Determination of velocity to various depth points is a direct result of the stacking process. The procedure is a simple one, long known to geophysicists, that consists of constructing right triangles based on varying ray paths from source to receiver off a common depth point. The triangle's equation is written in terms of measured times and distances with the average velocity of the interval above the depth point being the only unknown. Because the process involves taking a root of the squares of a number of terms, the resultant solution is referred to as the root mean square (RMS) or stacking velocity. Given the RMS velocities to a number of superimposed depth points, solving for interval velocities between depth points is a matter of simple arithmetic. Figure 11 is a presentation of a typical velocity analysis in the basinal sediments of Santaren Channel.The ordinant of this graph is scaled in RMS velocities in meters/sec. The abscissa is reflection time in seconds. At the top of the graph, a single curve gives a measure of reflection amplitude or reflectivity. Reflectivity maxima point up and minima

point down. Stacking velocities are determined at 0.1 second intervals and are indicated by vertical ticks marking the crestal position for the curve based at a given reflection time. Interval velocities are calculated between times at events that are reflectivity maxima, because these events tend to have greatest coherence and are most probably of greatest lithologic and time-stratigraphic significance. Sharp peaks on the velocity curves make it possible to pick velocities accurately down to reflection times slightly in excess of three seconds. Below three seconds, peaks of curves are generally obscure to nonexistant and velocities are picked mostly on the basis of trial and error to achieve coherent reflection events. It is important to keep in mind that RMS velocities to deeper events are increasingly inaccurate and these inaccuracies are passed on to determinations of interval velocities and depths.

Reflection Seismic Measurements

Mahlon M. Ball, Ray G. Martin,

Wayne D. Bock, and Richard Sylwester

In this part of our report, regional aspects of our study are described with reference to horizontally squeezed record sections that allow us to present all our data. These regional sections illustrate major structures and seismic-lithostratigraphic and time-stratigraphic units. Records at normal time scale are keyed to the squeezed sections and used to elucidate details of various features of interest. The initial figure presenting squeezed section data is labled with approximate values of vertical exaggerations.The horizontal scale of our time sections is 5 km to 100 shot points (SP). This means that vertical exaggeration is about 6 X for sea floor topography. The

upper second of sub-bottom section represents about 1 km of penetration. For this part of the record the vertical exaggeration is 3 to 4 X. One to two seconds down in the section represents 2 km of penetration with a vertical exaggeration of approximately 2 X. Below two seconds, interval velocities range upward from 5 to 6 km/sec and vertical scale is approximately equal to the horizontal scale. The frequency of data is around 25 to 30 cycles per second so the maximum dimension of a single cycle in the upper second of sub-bottom material approaches 40 m, Between one and two seconds, one cycle might represent as much as 80 m. Below two seconds, one cycle could represent as much as 120 m of section. In the case of one anticline with steeply dipping flanks, a migrated depth section with no vertical exaggeration is used to remove distortions that interfere with interpretations. The one-to-one migrated depth section is particularly important because it alone provides the standard by which readers can judge the misrepresentations unavoidably present in the vertically exaggerated and unmigrated time sections.

Figure 12 shows the squeezed section of line 1 (Figure 1). On the left or northern part of the profile, coherent reflections can be carried to the full length of the record, i.e. five seconds, which according to our velocity analyses represents a depth of about ten km. This uniform reflection character is typical of all of line 1 north of SP 2000. A ten kilometer broad, low relief anticline (Fig. 13) interrupts the monotony of the continuous and essentially flat reflections between SP 700 and 900. The feature has a relief of about 0.1 seconds or 200 meters on the mid-Cretaceous event. A number of amplitude anomalies occur over the crest of this structure. The feature appears to have affected the entire Cretaceous and older section and may be related to a deep flexure beneath its steeper southern margin. The same relatively flat and coherent reflection character is

11

present on lines 5, 6 and 7 (Figure 1) except at their ends where they are in close proximity to shallow bank edges. The strong reflection visible at 2.3 seconds (Figure 12) is traceable over the entire area of Santaren Channel north of the structure between SP 2000 and 2200. This event occurs at a depth of about three km, and based on correlations with lines farther north, tied to the Great Issac well at the northwest corner of the Great Bahama Bank, we believe the reflection marks a mid-Cretaceous event. Above three seconds (to a depth of about 5 km, which is approximately three times our source-to-far phone distance), moveout variations between primary reflections and multiples are sufficient to identify the reflections as primaries. Below three seconds, some multiples may occur, but in places several reflections are present that do not fit simple long-path multiple occurrences. We believe these reflections stem from velocity and density contrasts deep in the sediment section down to the full length of our recordings.

A main distinguishing feature of the structure between SP 2000 and 2200 (Figure 12, 14) is its location at an abrupt transition. On the north, continuous reflections occur to five seconds of reflection time. South of the structure, coherent reflections terminate at 1.3 seconds above a sequence of discontinous reflections that extend to about 1.8 seconds. Below 1.8 seconds, the section lacks coherent reflections. Other salient features of this structure include its breadth of about 10 km and its flank asymmetry. The north flank's maximum relief is about 1 km and that of the south flank is about 500 meters.

From the location of this structure relative to that described by Idris (1975) (Figure 6A) and the geometry of the reflections in both records, it appears that both lines cross the same structure. The earlier single channel data fail to emphasize its asymmetric nature. This failure is probably

12

the result of sub-bottom penetration of only 0.7 seconds above the seafloor multiple. A wedge of reflections is present in the single channel data on the south flank of the structure. In Idris's (1975) data (Figure 6A) coherent reflections were lacking in the core of the anticline. The multichannel line reveals a sequence of coherent reflections down to 1.8 seconds and a prominent amplitude anomaly on the top of the structure in the package of reflections that thins dramatically over the structural crest(Figure 14). This section thins three-fold over the structure.The thicker section is only weakly reflective off the structure and the thinner section whitens out completely on the crest with some abrupt terminations of reflections as they reach the whitened zone. A highly reflective contrast occurs at the top of the zone of reflections beneath the whitened zone. The upper section is unconformable on the lower as evidenced by packages of reflections that wedge out on this surface on both flanks of the structure (Figure 14) The highly reflective nature of the contrast across this unconformity apparently mirrored back essentially all single channel energy and prevented Idris (1975) from recognizing reflections below this surface. As a result, Idris (1975) incorrectly identified the material below the unconformity as shallow water carbonate platform rocks. The multichannel data on the other hand, through some combination of greater source energy, surpression of multiples and more effective AGC, show the reflection character of the material below the unconformity to be coherent and analogous to the inferred basinal carbonate material north of the structure. The multichannel data also indicate a deeper unconformity on the south flank of the structure where a zone of irregular but coherent reflections overlies a rough upper surface of a zone lacking coherent reflections. We infer this contact to record an upper zone of possibly tectonized basinal carbonate overlying shallow water carbonate platform

13

material. A ramplike configuration of reflections at 1.7 seconds between SP 1800 and 1950 (Figure 14) may represent material removed from the crest of the structure at the inferred unconformity and redeposited off the north flank of the structure.

A study of interval velocities together with the apparent correlation of the mid-Cretaceous reflection within the basinal sequence to the contact between irregular coherent reflections above the inferred platform carbonate rocks indicates the following approximate time stratigraphic assignments for the reflection sequences. The shallow reflection interval, above the whitened zone on the crest of the structure, has an interval velocity of about 2 km/sec. This interval is inferred to be Cenozoic deposits. The uppermost 0.2 seconds of weakly reflective material, on the crest of the structure, is inferred to be mostly Neogene. The package of strong and coherent reflections just above the whitened zone on the crest of the structure thins from 0.3 seconds to 0.15 seconds between the north flank and the crest of the structure. Terminations of events contribute to the thinning and take place in convergences suggestive of pinchouts on unconformable surfaces. This reflection character may represent erosional activity in the basin facies during Paleogene or early Neogene time. The whitened zone may represent Upper Cretaceous chalk. The interval of continuous reflections below the whitened zone has interval velocities ranging between 3 and 4 km/sec. We interpret this reflection package to represent impedance contrasts in Upper Cretaceous rocks. The contact at the base of this interval appears to correlate approximately with the mid-Cretaceous event in Santaren Basin toward the north and with the contact at the top of inferred carbonate platform rocks on the south. A few deep reflections extend from the north beneath the structure. In particular, the event at 3.1 seconds is strong, coherent and not readily

14

explained as a multiple. The depth at 3.1 seconds is approximately 6 km. The interval velocity between this event and the base of supposed Upper Cretaceous section is 5.8 km/sec. To the south, the section within this interval, where reflections are lacking, is probably Lower Cretaceous in age and perhaps contains even older platform carbonate rocks. Toward the north, where coherent reflections are plentiful, impedance contrasts in Lower Cretaceous and older basinal carbonate sediments are the probable source of the reflections. The apparent low .relief on the deep event coming from the basin to its position beneath the structure is in part an artifact of higher interval velocity.

We generated migrated depth sections at 1:1 and 2:1 ratios of vertical to horizontal scale in order to eliminate as much distortion as possible. The 2:1 vertical to horizontal scale (Figure 15) gave the best record quality for study of thickness variations. In the 1:1 section (Figure 16), the correct shape of the structure section appears compressed relative to its appearance in the time section (Figure 14). The undistorted section nearly eliminates the greater apparent structural relief on the crest at 1 second relative to closures at deeper horizons. No thinning on structure is apparent in the Lower Cretaceous and older sequences. The Upper Cretaceous, reflection package thins regionally from north to south across the structure. There is no localized thin on the structural crest within the Upper Cretaceous unit. Maximum loss of section is off the structure's south flank. The inferred uppermost Cretaceous and lower Cenozoic section thins by a factor of four across the crest. Upper Cenozoic sequences are twice as thick on the north flank and 20 to 30% thicker on the south flank than over the structure's crest. These thinning relationships indicate that the structure was formed near the end of the Cretaceous with maximum topographic relief in early

15

Cenozoic time. Late Cenozoic expression of the structure could be a result of increased compaction of thick semiconsolidated sediments on the flanks of the structure.

A number of distortions other than those introduced by velocity changes with depth are present in the time section over the structure (Figure 14). Dipping segments are plotted vertically below recording points. This places them downdip from their true position in the two dimensional record. Because lateral offsets of deeper dipping reflection are greater, the plotting error not only moves dipping segments downdip but also decreases apparent dip. Migration of the data over the structure (Figure 15) improved the correlation of events on the north flank of the structure.

The migrated section still retains the troubling cross over of the mid-Cretaceous event and the basal reflection of the inferred Upper Cretaceous sequence. The implication of this reflection geometry is that energy is arriving from out of the plane of the section for the deeper reflection over a distance of about 6 km on line 1 (Figure 15). The distance off line to this reflector from which the side echo is arriving is about 3 km. Thus, line 1 appears to be located close to the strike of the surface from which energy arrives from out of the plane of the section. On the basis of our knowledge of the location of the Idris (1975) crossing and the observed northwest dip on the extreme southeast end of line 4 (Figure 1); the western part of the structure appears to us to trend only slightly south of west at a high angle, approaching 90 degrees to the trend of line 1. The form of the eastern extension is unknown. Additional and more closely spaced lines with extension of coverage toward the east are needed to resolve apparent discrepancies.

A major structure (Figs. 17, 18) occurs at the eastern end of line 2 between SP 100 and 500. This feature has a steep eastern flank with a relief

16

of about one kilometer and a flank breadth of four kilometers (Figure 18).
Coherent reflections of inferred basinal carbonate sediments abut the core of
the structure This core lacks well defined reflections and is probably
composed of shallow water carbonate platform material. In the basinal section
adjacent to the structure's eastern flank (Figure 18) terminations and dip
changes indicate small normal faults with down to the east throws of tens of
meters. Diffractions and dip reversal at the base of this basinal section at
1.5 seconds indicate that the eastern flank may be fault controlled. Faults
die out in the early to mid-Cenozoic section and the more or less
structureless Neogene sequence blankets the older basinal section. The
basinal sediments on the 20 km long sloping western flank of the structure
onlap the structureless core from a depth of one kilometer to the crest which
is only 300 meters subbottom. The length of the western slope is 20 km. The
surface of the inferred shallow water platform block is rough with
protuberances over 100 meters high with apparent widths of about a
kilometer(Figure 18). These dimensions are suggestive of the karst hills
known as mogotes developed on carbonate terranes at various places in the
Greater Antilles. From the track chart of Idris (1975) it is clear that the
second structure he encountered on a NNW-SSE crossing (Figure 6) also is
present on the eastern end of line 2 on an E-W crossing. The steeper flank in
the Idris (1975) crossing dipped north. Therefore, to judge from both
crossings, true dip of the steep flank is toward the northeast.

On the west, line 2 consistently shows a weakly-reflective Neogene
section at the top. It overlies a sequence of high amplitude, discontinuous
reflections that mark seismic impedance contrasts in basinal Upper Cretaceous
and lower to middle Cenozoic rocks (Figure 17). The underlying deposits,
inferred to be carbonate platform rocks of Early Cretaceous age, have a rough,

highly reflective surface but no well defined internal reflections. At SP 900 (Figure 17), a graben is present. The graben's faults offset the top of Lower Cretaceous rocks 100 meters. The breadth of this structure is about 2.5 km. Offsets of tens of meters are apparent in the overlying Upper Cretaceous and Early Cenozoic sequences. The upper Cenozoic weakly reflective unit is unaffected by the faults. Farther west, some channelling is apparent on the sea floor, and some structures suggestive of buried channels and unconformable surfaces are present in the sediments of late Cretaceous and early to middle Cenozoic age.

Near the western end of line 2, at SP 3500, the top of the inferred Lower Cretaceous section peaks at 0.8 seconds subbottom in a two kilometer broad ridge with a basinward, western slope extending down to 3 seconds (Figure 17). Reflective basinal section onlaps the seaward slope. We believe the ridge and slope mark the location of a Lower Cretaceous Platform edge. The material lacking coherent reflections below three seconds west of this edge may be an even older more extensive Cretaceous or Jurassic carbonate platform.

Line 3 (Figure 19) is similar to Line 2. At its eastern end, probable Lower Cretaceous shallow water carbonates are rising in the long western slope of the tilted platform block seen at the eastern end of line 2. The overlying basinal carbonates, containing coherent reflections, onlap the deeper surface. The sequence is capped by a weakly reflective Neogene basinal unit. Small faults offset the Lower Cretaceous surface and the overlying reflective beds. These are visible between SP 3100 and 3300 and at SP 1430. The reflective basinal section contains apparent broad surfaces of erosion with onlapping sequences wedging out on reflections marking unconformities. Channels are apparent on the seafloor and configurations of reflections within

18

the subbottom are suggestive of channel fills and mounded sediment bodies. The platform edge at the west end of line 3 (Figures 19 and 20), is even better depicted than on line 2. The breadth of the ridge at the slope break is 2 to 3 km. The ridge has a relief of about 100 meters over the backreef or platform interior surface. The relief of the platform edge over the floor of the adjacent basin appears to be at least a kilometer. The angle of declivity of the slope approaches 20°. The deepest coherent reflections in the basin sequence are at a depth of about 3400 meters with a thickness of the basinal section of about 2 km (Figure 20).

The southeastern end of line 4 (Figures 21, 22) appears to cross the west end of the structure seen near the south end of line 1(Figures 12, 14). The central portion of the line also reveals several onlaps and truncations indicating erosional events in the basinal sequence overlying the inferred carbonate platform rocks. The top of carbonate platform rocks is difficult to impossible to recognize in the southeasternmost portion of line 4. We believe the surface of platform carbonates to be at 2.2 seconds near SP 250 (Figures 21 and 22). It is traceable westward beneath coherent reflections of onlapping Upper Cretaceous basinal section. Truncations within the Upper Cretaceous unit are indicated at 1.7 seconds between SP 340 and 500 (Figures 21, 23). The reflective Upper Cretaceous unit pinches out near SP 560 (Figure 23). A weakly reflective section of youngest Cretaceous to early Cenozoic age onlaps the platform rocks and pinches out at SP 630. This corresponds to the whitened zone over the structure at the south end of line 1. Terminations of dim events at the top of this unit are apparent between shot points 430 and 540. West of shot point 630, the buried platform material is onlapped by the strongly reflective unit inferred to be of early to middle Cenozoic age. The uppermost unit of weak reflections is the capping Neogene basinal sequence.

The surface of the zone of no reflections inferred to represent the top of shallow water platform rocks rises in the section toward the west (SP660-720) and is onlapped by successively younger basinal units in that direction. The inferred platform surface can be traced farther westward, beyond the end of line 4, to the point where it crops out on the seafloor and rises to form the slope of the present-day Cay Sal Bank (Figure 21). At this location, the reflector is of Recent age, strongly suggesting the platform surface is time transgressive from at least the Early Cretaceous to the Recent.

Line 5 (Figure 24, 25) contrasts sharply with line 4. At the western end of line 5, a deep zone of no reflections appears as a block below 2 seconds. The block of platform material ends abruptly near SP 70 where continuous reflections of the basinal section terminate at a steeply dipping contact (Figure 25). Diffractions, terminations and dip changes at the contact indicate the presence of a fault. This fault appears to have affected the entire youngest Cretaceous to middle Cenozoic section below 1.1 seconds. East of the platform-to-basin transition, highly reflective basinal carbonates occur to the full recording time of three seconds (about 5 km). The Mid-Cretaceous event stands out at 2.3 seconds. A dip reversal with a breadth of almost 10 kilometers and relief of less than 100 meters on the mid Cretaceous event occurs between SP 360 and SP 540 (Figure 24). Relief on this feature is expressed up to and including the seafloor.

Lines 6 and 7 (Figures 26 and 27) are similar in character to line 5. The entire sections seen on these lines contain coherent reflections of the probable basinal carbonates. The mid-Cretaceous event can be correlated over the full extent of these lines. Apparent anticlines near both ends of line 6 are suspect because they occur in turns off of and onto adjacent lines. A dip

20

change at SP 250 on line 6 (Figure 26) appears to affect the entire sediment section and may be related to faults below the 5 km thick section seen on this line.

Gravity and Magnetic Measurements

Mahlon M. Ball, Robert M. Bowles,

Lewis Gilbert, and Elizabeth L. Coward

The potential field data (Figure 28) acquired along our seismic lines are too sparse to map. They nevertheless supply important constraints on the interpretation of the seismic data. The magnetic anomalies are of long wavelength and few paired positive-negative reversals occur on any of our lines, indicating that depth to magnetic basement is exceedingly deep in Santaren and Nicholas Channels.

The gravity data show an eight milligal positive edge effect across the transition at the site of the junction of basinal sediments of Santaren Channel with the inferred Lower Cretaceous shallow water carbonate platform rocks at the south end of the line 1. This anomaly is not localized on the anticlinal structure at SP 2000-2200. Instead, it appears to reflect the positive density contrast of the shallow water carbonate platform rocks to the lower density basinal sediments toward the north. A positive anomaly of 12 milligals is associated with the tilted block of inferred platform carbonate material at the east end of Line 2. Allowing for a 0.3 gm/cm^3 density contrast between the platform carbonates and the surrounding, less dense basinal carbonate material, an anomaly is calculated that closely matches the observed anomaly. Again we believe the anomaly stems from juxtaposition of dense Lower Cretaceous carbonate platform rocks with onlapping basinal sediments of Late Cretaceous age. Neither of these features has an associated

21

magnetic anomaly. This lack of magnetic expression is consistant with the idea that dense platform carbonates core both these structures and that no igneous or metamorphic rocks are present at shallow depths in either feature.

Discussion

Mahlon M. Ball, Ray G. Martin,

Wayne D. Bock and Richard Sylwester

Our measurements reveal the. northern edge of Bahaman carbonate masses involved in the Cuban collision. The anticlinal structure between SP 2000 and 2200 on line 1 (Figures 12, 14, 15, 16) occurs at this point. Our data over this feature constitute our sharpest image of this contact. These data are, nevertheless, difficult to understand. A transition from a topographic basin to a shallow water platform agrees in position with the anticline and dictates that a depositional structure, that is, a platform edge and slope, should be recognizable at this location. No such feature is readily discernible. One might argue that, because the surface of the inferred platform is rough and possibly has been subjected to erosion and karstification, the depositional structure has been destroyed. In fact, the general tendency seems to be for erosion to modify platform edges and slopes in such a manner that they become oversteepened, because the angle of declivity on these features commonly exceeds any possible angle of repose. The asymmetric folding of strata into an anticline above the transition is best explained as a result of compressional tectonism. This poses the question: has the compressional tectonism in some way masked the erosional-depositional structure of the elevated platform edge rim and slope?

An additional complication revolves around the anomalous thickness variations in the largely Upper Cretaceous section bowed up in the

22

anticline. These strata thin from 1.5 km on the north, in Santaren Channel, to 1.1 km on the structural crest (Figure 15). Much of this thinning appears to result from erosion on the structural culmination. The most dramatic thinning in the sequence is on the south flank of the structure where upper units that thicken southward off the structural crest abruptly converge (at SP 2200) to a miniscule vertical dimension of only 600 m. Significant dip changes do occur at the locus of the abrupt thickness transformation, but there is no other clear cut indication of faults at this point. Deep terminations below four km in inferred basinal sediments, beneath the anticline, are offset three km northward from the site of the dip and thickness variations. It is conceivable that some major dislocation related to faults caused the aberrant dips and thickness variations.

What is most clear is that the northern edge of the Bahaman carbonates disrupted by Cuban tectonism does not look like a typical arc - trench system where competent crust overrides relatively incompetent oceanic crust. In reflection records, this family of plate boundaries reveals some indication of a subducting plate overlain by a melange of sediment containing counterregional dipping reflections interpreted to represent thrust fault planes (for examples see Hamilton, 1977, Figs. 5, 6, 8, and 12). Our crossing of the northern edge of the Bahaman Cuban collision zone appears more like the asymmetric anticlinal features seen in dip sections across the leading edges of the Cordilleran overthrust belt. If this analogy is meaningful, we must postulate that the thick basinal carbonate section in Santaren Channel, which may overlie oceanic crust, behaves in a competent manner analogous to thick continental crust in the overthrust belt. Both the great thickness and high interval and refraction velocities noted at relatively shallow depths in Santaren Channel are consistent with this speculation.

In a more positive vein, the timing and sequence of events deduced from onshore geology in Cuba easily accomodates a fit with observations from our data. Assuming the validity of our pick of the mid-Cretaceous reflection event and its approximate correlation with the top of one level of shallow water platform carbonate rocks, the structure observed offshore appears to have been formed in late Cretaceous and early Cenozoic time. The major unconformity indicated by truncation of events in the crest of the structure and synchronous pinchouts of onlapping strata on its flanks appear to occur near the Cretaceous-Cenozoic boundary. Discordances and conglomerates are abundant in onshore well data at the Cretaceous-Cenozoic boundary (Pardo, 1975). The rough nature of the inferred top of Lower Cretaceous platform rocks and the marked change in reflection character across this contact indicate that this surface also is a major unconformity. The presence of evaporites in the section tends to corroborate this inferrence. Independent lines of evidence supporting the unconformable nature of both the Upper and Middle Cretaceous surfaces are the marked increases in interval velocity across both events. These increases are responsible for the strong reflectivities of these surfaces.

Our data do not provide evidence regarding the possible influence of left-lateral strike-slip faulting in the collision zone. Such activity is however implied by current interpretation of pre-Eocene plate motion and is consistent with onshore geology in Cuba. Figure 29 shows major tectonic features of the island. The major-strike slip fault along the north coast, constitutes the south boundary of the carbonate belt on the north coast. Note the near perfect fit in sense and trend of second order shears on the strain ellipse section, included in Figure 29, to the orientation of left-lateral and right-lateral, second order, strike-slip faults crossing and offsetting the

24

Cuban arc.

The larger question, concerning what our data reveal bearing on the history of what has been referred to as the Caribbean-North American paleoplate boundary, has only a subjective answer. Mainly, we are forced to recognize that this boundary is a broad zone rather than a well-defined line. Our interests have been focused on a band, narrowed by overthrusting, extending from the south margin of the north coast carbonate belt to the northern edge of disrupted carbonates at the junction of Santaren and Nicholas Channels. This band currently spans a N-S width of about 100 km, a small part of what the paleoplate boundary must have encompassed. Based on correlation of geophysical and geological data, Klitgord and Popenoe (in press) infer fracture zones comprising the boundary to have extended across a width limited by Campeche Bank on the SW and Lake Okeechobee, in Florida, on the NE, a distance of approximately 550 km. Cuba has apparently overriden this ancient boundary zone by about half its width. The present Caribbean has a north-south dimension of about 1000 km. The portion of the Atlantic offsetting the Caribbean to the east is the locus of a phalanx of fracture zones with attending left-lateral offsets of topography and potential field data (Ball and Harrison, 1969). At the northern end of the Lesser Antilles the Atlantic fracture zones merge with the eastward projection of the fractures picked by Klitgord and Popenoe (in press). From this, it does not seem unreasonable to speculate that what has been referred to as the North American - Caribbean paleoplate boundary is in fact the northern part of a pre-Eocene boundary zone that extended all the way to South America. Thus the ancestral Caribbean was a zone of north-south extension and left-lateral shear between the American Plates (Ball and Harrison, 1969, 1970). Only after the early Eocene, with the formation of the Lesser Antilles Island Arc and the Cayman Trough can the

25

Caribbean properly be referred to as a plate with North and South American boundaries.

Tilted blocks of inferred shallow water carbonate platform materials (Figures 6, 17, 18) constitute a class of structure related primarily to tectonism in the Cuban collision zone of the Bahamas province. The upper surface of these blocks is clearly eroded and onlapped by Upper Cretaceous and Cenozoic basinal carbonate sediments. The observed history of movement of these blocks (Figure 6) appears similar to that of the anticlinal feature at the south end of line 1. That is, Upper Cretaceous to Cenozoic strata are bowed upward on the apparently fault controlled flanks of these features. A major difference appears to be that the basinal section either did not overlap the blocks prior to their uplift or, if such overlap did exist, it was subsequently removed by erosion; for the blocks lack any substantial section of upward arched basinal materials over their crests. Our observations do not rule out the possibility that the blocks and the anticline are end members of a continuum. The occurrence of a well defined positive gravity anomaly over the blocks argues against their origin being related to upward arching over salt pillows, and instead, favors compressional tectonism.

Another intriguing aspect of the inferred basinal section overlying the carbonate blocks is its relative lack of coherence as compared to the basinal section in Santaren Channel to the north. Irregular compaction over the rough surface of the underlying platform carbonates in Nicholas Channel may in some degree explain the noncoherent character of overlying reflectors. Some of the rough surface of the underlying platform rocks may be related to faulting which is undetectable in the platform materials due to a lack of internal reflections. Erosion related to influx of sediments from surrounding platforms would be no less effective in Santaren Channel than in the Nicholas

26

Channel. An exception to this statement might be related to Cuba's role as a sediment source in Nicholas Channel but the lack of terrigenous clastics in the northern Cuban carbonate section would seem to rule out this possibility as an explanation for increased roughness of the Nicholas Channel reflectors.

Depositional structure related to the occurrences of reefs or platform edge-slope complexes within the Cuban-Bahaman contact zone are clearly identifiable in the western reaches of Nicholas Channel (Figures 17, 19, and 20) and are logically inferred .at the transition of basinal to platform carbonates in southern Santaren Channel. If our speculations on age are correct, it follows that the Lower Cretaceous platform edge embays some distance toward the north in the Florida Straits with an arm of deep basin branching off the Straits toward the southeast in Santaren Channel (Figure 30). Earlier interpretations of the distribution of this platform edge (Figure 30), based on less information, quite logically carried the Lower Cretaceous reef southeastward from the last known occurrence on the southern slope of the Florida peninsula to the outcrop area of northern Cuba. Our new data suggest a more complicated picture. Indeed, using the isolated platform masses of the southeastern Bahamas as a model and considering the occurrence of both basinal and platform carbonates in northern Cuba, it seems likely that distribution of Lower Cretaceous platform edges in this region could well be complicated to a degree that defies complete reconstruction.

Regarding exploration potential of the collision zone for oil and gas, structures are present with favorable configurations and attractive sizes for formation of hydrocarbon traps in drillable water depths, ranging between 500 and 1000 meters. The compressional anticline noted at the south end of Line 1 has an apparent width of ten kilometers. If this breadth is a true diameter of a subcircular structure, its area of closure would be approximately 30

27

square miles. Assuming a 100 ft. pay thickness, 12.5% porosity, a water saturation of 25%, a formation volume factor of 1.45 and a recovery factor of 40%; this closure would contain approximately 400 x 10^6 recoverable barrels of oil. The volume of gas; assuming an ideal gas trapped in a similar area of closure, pay thickness, porosity and water saturation with a recovery factor of 0.8 and a reservoir temperature of $100^{\circ}F$ (seafloor temperature of $50^{\circ}F$ and a thermal gradient of $1^{\circ}F/100$ ft at a subseafloor depth of 5000 ft.); would be one trillion six hundred billion cubic feet at one atmosphere and $60^{\circ}F$. The tilted blocks of platform carbonates form even larger structures and if they were buried to greater depths would constitute even larger closures. The two possible salt structures noted in our regional coverage plus the occurrence of salt diapirs onshore in Cuba opens the potential for salt structures in this vicinity. The combination of depositional and erosional structure present along the platform edges in this area also represent potential stratigraphic traps. Finally, the wealth of unconformities coupled with wedging out of onlapping sediments offer potential for stratigraphic pinchouts.

Reservoirs and seals would seem likely to be plentiful in both the basinal and platform carbonates. Where the basinal section has consolidated and has been subsequently bowed upward in compressional structures, there is the potential for development of fracture porosity. It also seems likely that burial depths of basinal section on anticlinal crests have not been too excessive for preservation of some original porosity in chalky strata. Where uplift has been attended by erosion of the deep water section another possible means of enhancing porosity and permeability exists. Overlying unconsolidated oozes lack permeability and could provide adequate seals. Solution activity and dolomitization are both common processes active in platform rocks and

could lead to good reservoir qualities. Seals provided by bedded evaporites

and tight carbonates are common in onshore wells of northern Cuba and in the

deeper part of the carbonate section drilled on Cay Sal.

The conditions of source, maturation and migration of petroleum for

northern Cuba and the southwestern Bahamas seem favorable for commercial

hydrocarbon occurrence. The black limestones mentioned in the onshore wells

and outcrops of Cuba may be potential source rocks. Oil seeps occur onshore

and some small amounts of production have been achieved. The extreme

thicknesses of sediment, with estimates ranging in excess of ten kilometers,

argue that even the lowest thermal gradients would create subsurface

temperatures adequate to mature source rocks to the extent that they would

expel oil and gas. Faults, so commonly encountered in wells on the north

coast of Cuba should provide routes for migration of petroleum into traps.

Finally, the occurrence of amplitude anomalies such as those present on the

crest of the anticline at the south end of line 1, associated with flat

reflections underlying local closures, may be direct evidence of gas and gas-

liquid contacts. These features will undoubtedly be tested in the future.

FIGURE CAPTIONS

Figure 1. Index map with bottom topography contoured in meters from Sorenson
and others (1975). Well depths are in meters. Fine lines
numbered 12,17,19,21,24,26,and 27 designate CDP seismic lines
described in this paper. The numbers refer to figures in which
squeezed sections of entire lines appear. Thick bars represent
detailed time sections of portions of these data. Numbers refer
to figures in which sections, indicated by the bars, are shown.
Sticks with capped ends numbered 5, 6A and 6B show locations of
single channel lings from Idris (1975). Again, numbers refer to
figures where these data are shown.

Figure 2. Geologic map and cross section from Meyerhoff and Hatten (1968)
showing major structural features of onshore Cuba adjacent to our
offshore study area.

Figure 3. Local geologic map and cross section from Meyerhoff and Hatten
(1968) showing the nature of a salt diapir in the north coastal
zone of Cuba adjacent to our offshore study area. See Figure 2
for location of this feature.

Figure 4. Time and lithologic stratigraphy of available wells in Cuba and
Cay Sal. These data are taken from compilations of oil company
data by Furrazola-Bermudez and others (1964) and Tator and
Hatfield (1975 a and b). Symbols are as follows; J_1; early
Jurassic, J_2: middle Jurassic, J_3: late Jurassic, C_1: early

Cretaceous, C_2:   late Cretaceous, Pg: Paleocene, N = Neogene,

Tr: Teriary. Lower case letters stand for Cretaceous stage names

as follows; h: Neocomian, ap: Aptian, al: Albian, cm:

Cenomanian, cp: Campanian, m: Maestrichtian.

Figure 5.   A possible salt diapir (from Idris, 1975) just southeast of Cay

Sal at 5 on Figure 1. These data were collected using a 40 in.^{3}

airgun system.   Vertical exaggeration in the sediment section is

approximately 10X.

Figure 6.   Structures revealed by single channel, 40 in^3, airgun data from

Idris (1975).   These structures are located at 6A, and 6B in

Figure 1. The small anticline at 1.7 seconds depth near 0930 at

the left of 6B may be a result of diapirism. The two structures

seen in 6B are separated by a course change and may represent a

single block bounded by a fault scarp on the north and east.

Figure 7.   General flow for U.S. Geological Survey common depth point

processing.

Figure 8.   Diagrammatic flow chart of the processing steps used to generate

the migrated time and depth sections from the scaled stack data.

Figure 9.   Iso - velocity plot of the unsmoothed stacking velocities.

Figure 10.   Iso-velocity plot of the smoothed stacking velocities used to

convert the migrated data from time to depth.

Figure 11. Here, an example is shown of velocity analysis performed in

processing done by Phillips Petroleum Company in the creation of

the time sections on which this report is based. The salient

features of this presentation are the two graphs occupying the

lower right portion of the figure. The abscissa of both these

graphs are reflection times. The ordinate of the upper graph is a

measure of reflection strength with positive values making upward

excursions. The positive peaks on this curve mark the reflection

time of occurrence of strong reflections. The ordinate of the

lower graph is a log scale expressing RMS velocities. The family

of curves climbing toward the right from 0.8 to 3.0 seconds of

reflection time has peaks opposite the RMS velocity that achieves

the best correction of moveout at the specific reflection times.

This best fitting velocity is the stacking velocity for that

reflection time in the CDP processing. The flat portion of each

curve lies on a vertical that marks the time of reflection

occurrence. For example, the seafloor reflection occurs at 0.8

seconds. It is marked by a strong positive excursion at 0.8

seconds in the upper graph. In the lower graph, a peak occurs

opposite the RMS velocity of 1500 meters/sec at the reflection

time of 0.8 seconds. Thus, as one would expect, the transmission

velocity of seismic energy in water, i.e. 1500 meters/sec, gives

the best moveout correction for the sea floor event and this

velocity is used in the stacking process for the reflection

occurring at 0.8 seconds. Note the poor definition of peaks

marking stacking velocities below 3.0 seconds reflection time.

This time corresponds to depths roughly three times streamer

length. At this depth, moveout variation across the phone spread has decreased to the point that accurate moveout corrections are indeterminable and large errors in velocity determination may result(Personel communication, Fred Barmwater). The tables on the left consist of the upper two that serve to identify records and location of data and a lower one with calculations of RMS velocities, depths, and interval velocities between strong reflections. The choice of strong reflections as limits for interval velocity determinations creates an optimum possibility that the interval velocities will have lithologic significance.

Figure 12. The purpose of this horizontally squeezed time section of Line 12 (See Figure 1 for location) is two-fold. First, resulting vertical exaggeration enables detection of subtle structures and second we are able to present all our data without resorting to use of line drawings that eliminate consideration of amplitude anomalies and force readers to proceed at the mercy of authors with no capability to exert quality control regarding seismic interpretations. In this and succeeding sections, north and west are on the left. Shot points (SP) are indicated at the upper margin. One hundred SP equals five kilometers. The vertical scale is in seconds. A few prominent reflections are marked and tentative stratigraphic horizons are indicated. MKE is an inferred mid-Cretaceous event. TLK is the inferred top of lower Cretaceous rocks. TK is inferred top of Cretaceous rocks and TP is the inferred top of the Paleogene section. Approximate vertical exaggerations are indicated for succeeding one second

33

intervals of subbottom penetration. The coherent character of reflections to the full recording time of 5 seconds north of SP 2000 are believed to mark velocity and density contrasts in the basinal carbonate sediments of Santaren Channel. A large anticline (10 kilometers broad) occurs at the transition from continuous reflections at depth to a zone lacking coherent reflections below 1.8 seconds. The zone of no reflections is attended by a positive gravity anomaly and has no magnetic signature. For these reasons, this reflection character is inferred to result from presence of shallow water carbonate platform rocks. Locations of related figures providing details of significant local structures are indicated in the upper margin.

Figure 13. Enlarged segment of Line 1 showing a broad low relief dip reversal that occurs between SP800 and 900. Apparent relief on this crossing is 100 to 200 meters; breadth is five to ten kilometers. The feature may result from flexure over a deeper fault.

Figure 14. Time section of the southern end of Line 1 showing the nature of the transition from inferred basinal carbonate strata to essentially reflectionless carbonate platform material of inferred early Cretaceous age near the confluence of Santaron, Nicholas and Old Bahama Channels. The broad anticline, between SP 2000 and 2200, occurs above the abrupt contact. The north flank of the structure has a relief of about one kilometer and the south flanks' relief is about 500 meters. The surface of the zone of no reflections south of the structure is at 1.8 seconds. This surface

is rough and is inferred to represent a karstified unconformity on Lower Cretaceous platform rocks. Upper Cretaceous basinal carbonate rocks characterized by continuous reflections, are arched up over the structure. The surface of this sequence is also an unconformity with truncation of reflections apparent between SP 2150 and 2200. Maximum thinning over the structure occurs in the zone of poor reflections overlying the unconformity. This zone is inferred to be composed of uppermost Cretaceous and early Cenozoic chalks. The band of strong reflections capping the chalks is thought to result from lithologic contrasts associated with unconformities in a basinal carbonate section of largely Paleogene age. The capping zone of poor reflections is believed to be Neogene basinal carbonate sediment.

Figure 15. This migrated depth section of Figure 14 at a vertical exaggeration of 2X, shows good continuity of deep basinal reflections beneath the anticline overlying the basin-to-platform transition. The cross over of the mid Cretaceous event and the basal reflection of the basinal carbonates arched over the structure remains after migration and must result from side swipe of local subsurface sturcture at the northern margin of the anticlinal feature.

Figure 16. This 1:1 vertical to horizontal migrated depth section of Figure 14 shows the true configuration of the assymetric anticline above the Lower Cretaceous carbonate basin-to-platform transition.

35

Figure 17. This squeezed seismic section of Line 2 extends for 200 kilometers in Nicholas Channel between Cay Sal and Cuba. The line reveals an Upper Cretaceous and Cenozoic section onlapping inferred Lower Cretaceous platform carbonates from west to east. An unconformity occurs at the surface of the zone of no reflections thought to represent Lower Cretaceous platform material. Reflection terminations and convergences are the basis for inferring a number of unconformities in the basinal section onlapping the deep zone of no reflections. A large buried fault bounded block of platform material underlies the eastern end of the line. The western edge of the platform lies beneath SP 3500.

Figure 18. This time section of a segment of Figure 17 shows a block of shallow water platform material onlapped by younger Cretaceous and Paleogene basinal carbonates and capped by Neogene basinal carbonates at SP 300 at its shallowest point beneath the seafloor. This block is more than 20 kilometers broad and has a steep east slope with a kilometer of relief over a horizontal distance of three kilometers. Reflections terminating against this slope are marked by dip changes and obscured by diffractions; it follows that the slope may be a fault scarp. The block has an associated gravity maximum of 12 milligals and no magnetic signature. The surface of this platform block is rough with protuberances whose heights are approximately 100 meters with widths of about one kilmeter. These dimensions are reminicent of karst hills (Mogotes) seen on limestone terrains onshore in Cuba and Puerto Rico.

Figure 19.   This squeezed section of Line 3 is similar to that of Line 2. A
             platform edge occurs at the west end of the line. This feature is
             shown in detail in Figure 20. The inferred Lower Cretaceous
             platform rocks lack internal reflections and have a highly
             reflective, rough surface. The overlying basinal carbonates of
             inferred Late Cretaceous age onlap this rough surface from west to
             east. Unconformable surfaces are apparent in these basinal
             sediments. The overall continuity of reflections in the younger
             basnal section is less striking than in Santaren Channel.

Figure 20.   Time section of the western end of Line 3 showing configuration of
             the platform edge beneath SP 200. The edge has a relief of about
             one kilometer over the adjacent basin to the west and spans a
             horizontal distance of about four kilometers. The highest portion
             of this bank margin appears to be as much as 200 meters above the
             surface of the platform interior, shallow water carbonates toward
             the east. Reflection character and interval velocity
             determinations are the basis for the time stratigraphic picks
             shown in the record margin.

Figure 21.   This squeezed section of Line 4 shows the onlapping nature of
             basinal carbonate sediments off the southeastern tip of Coy Sal
             Bank. The steep westward dips at the east end of this short line
             mark the western margin of the structure seen between SP 2000 and
             2200 on Line 1 (Figures 1,12, 14-16). Details of the onlapping
             section of either end of the line are shown in Figure 22 and 23.
             The western portion of Line 4 consists of a clearly defined set of
             onlapping basinal carbonates abutting and burying a rough surface

of high reflectivity that is inferred to be the top of shallow
water carbonate platform rock. Beyond the western end of the
line, this surface crops out on the seafloor and rises to the sea
surface where it is exposed as the face of Cay Sal Bank. This
surface thus transgresses geologic-time from Early Cretaceous in
the eastern portion of line 4 to Recent on Cay Sal Bank.

Figure 22. The eastern end of Line 4 (Figure 1) showing a zone of steep
westward dip at the edge of the figure. These dips mark the west
edge of the anticlinal structure seen between SP 2000 and 2200 at
the south end of Line 1 (Figure 14).

Figure 23. The onlapping character of the younger Cretaceous and Cenozoic
basinal carbonates overlying inferred platform rocks is evident in
the western part of line 4. Some terminations of reflections
occur near the top of the younger Cretaceous section beneath SP
500. Small faults may be present beneath SP 570 and 680.

Figure 24. This squeezed section of Line 5 shows the coherent character of
reflections from the basinal carbonate section in Santaren
Channel. Figure 25 shows details of the zone of dip changes and
the roll-over structure near the west end of this line. Apparent
throw on the fault inferred to cause this structure decreases with
depth.

Figure 25. The western end of Line 5 seen in this time section shows a deep abrupt contact of a seismic unit lacking internal reflections with the coherent reflections of the basinal carbonates in Santaren Channel. Terminations and dip changes indicate the contact is the locus of a high angle fault that extends upward to 1.4 seconds near the top of the inferred Cretaceous section. The apparent slight decrease of offset on the fault and relief of associated roll over at increased depth favor the likelihood of strike-slip displacement on this feature.

Figure 26. This NW-SE oblique crossing of Santaren Channel on Line 6 emphasizes the continuous nature of the reflections associated with the basinal carbonates infilling the channel. Apparent structures at the edges of this record may be artifacts of turns off and onto connecting lines.

Figure 27. The squeezed section of Line 7 also reveals the exceptional continuous nature of reflections in the Santaren Channel subbottom. This continuity is better developed than that seen in the inferred Upper Cretaceous and Cenozoic basinal section in Nicholas Channel (Figures 17 and 19).

Figure 28. Potential field data are shown with time and shot point numbers along track lines. Circled figures are line numbers. Numbers in 500 unit intervals are shot points. Small numbers in brackets are times. Numbers with one decimal place are free air gravity anomalies computed using the Gravity Formula for the Geodetic Reference System, 1967. Numbers in parentheses are total field

magnetic anomalies. Only the last three digits are shown for 46000 gamma values. Where values rise above 47000 all five digits are shown.

Figure 29. Structural diagram of Cuba after Rigassi (1961, Figure 1). The salient features of this figure are the first order, left-lateral strike-slip fault along the north coast of Cuba and the related sets of second order NE-SW left-lateral strike-slip faults and NNW-SSE right-lateral strike-slip faults that cross the island. The strain ellipse section idicated the inferred second order fault orientations related to the controlling left-lateral fault along Cuba's north coast.

Figure 30. Inferred Lower Cretaceous Reef Trends (after Meyerhoff and Hatten, 1974, Figure 5). The dashed line indicates the trend as envisioned by Meyerhoff and Hatten. The northward extension into Florida Straits and Santaren Channel indicates a more complicated platform edge distribution necessitated by new information presented in this report.

REFERENCES

Ball, M.M. and Harrison C.G.A., 1969, Origin of the Gulf and Caribbean and Implications Regarding Ocean Ridge Extension, Migration and Sheer. Transactions - Gulf Coast Association of Geological Societies, v. 19, p. 287-294.

Barmwater, Fred. 1981 (Personal Communication).

Ducloz, C. and Vuagnat, M. 1962, A propos de l'age des serpentinites de Cuba: Geneve, Archives Science, Societe, Physique, Historique, Naturel, v. 15, pt. 2, p. 309-322.

Furrazola-Bermudez, Gustavo, Judoley, C.M., Mihailovskaya, M.S., Miroliubou, Y.S., Jimenez, A.N., and Solsona, J.B, 1964, Geologia de Cuba. Institute Cubano de Recursos Minerales, p. 1-239.

Hamilton, Warren, 1977, Subduction in the Indonesian Region, in Talwani, Manik, and Pitman, W.C. III eds., Island Arcs, Deep Sea Trenches and Back Arc Basins. Maurice Ewing Series 1, p.1-470. American Geophysical Union, Washington, D.C., p. 15-31.

Idris, Faisal M. 1975, Reflection seismic measurements in the Old Bahama Channel north of Cuba: M.S. Thesis, Univ. of Miami, Fla., p. 1-41.

Klitgord, K.D., Popenoe, Peter, and Schouten, Hans, in press, Florida: A Jurassic transform plate boundary. Journal Geophysical Research.

Mattson, P.H., 1973, Middle Cretaceous nappe structures in Puerto Rican ophiolites and their relation to the tectonic history of the Greater Antilles. Geological Society of America Bulletin, v. 84, p. 21-38.

Mattson, P.H., ed. 1975, West Indies Island Arcs: Benchmark Papers in Geology. Stroudsburg, PA, Douden, Hutchinson and Ross, p. 1-400.

41

Meyerhoff, A.A. and Hatten, C.W., 1968, Diapiric Structures in Central Cuba, in Diapirism and Diapirs, American Association of Petroleum Geologists Memoir 8, Braunstein, Jules and O'Brien, G.D., eds., p. 315-357.

Meyerhoff, A.A. and Hatten, C.W., 1974, Bahamas Salient of North America: Tectonic framework, stratigraphy, and petroleum potential: American Association of Petroleum Geologists Bull. v. 58, p. 1201-1239.

Pardo, Georges, 1975, Geology of Cuba, In, Nairn, A.E.M. and Stehl, F.G., 1975, eds. The Gulf of Mexico and The Caribbean, Ocean Margins and Basins, Vol. 3, p. 1-706, New York Plenum Press, p. 553-615.

Rigassi, D., 1961, Quelque Vues Nouvelles sur la Geologie Cubaine: Chron. Mines et Recherche Miniere, 29, p. 3-7.

Sheridan, R.E., Drake, C.L., Nafe, J.E. and Hennion, J., 1966, Seismic-refraction study of continental margin east of Florida: American Association of Petroleum Geologists Bull., v. 50, p. 1972-1991.

Sorensen, F.H., Snodgrass, L.W., Rebman, J.H., Murchison, R.R., Jones, C.R. and Martin, R.G., 1975, Preliminary bathymetric map of Gulf of Mexico region: U.S. Geological Survey Open File Report 75-140.

Tator, B.A. and Hatfield, L.E., 1975, Bahamas Present Complex Geology Pt. 1, Oil and Gas Journal, Oct 27, p. 172-176.

Tator, B.A. and Hatfield, L.E., 1975, Bahamas present complex geology, Pt. 2, Oil and Gas Journal, Nov. 3, p. 120-122.

Wassall, 1957, The Relationship of Oil and Serpentine in Cuba: 20th International Geological Congress, Mexico, Proceedings Section 3, p. 65-77.

MIAMI

Bimini
Islands

Cape Sable

WILLIAMS
TD 3648

GREAT BAHAMA BANK

STATE
826Y
TD 4717

FLORIDA

BIG PINE KEY
TD 4717

Pourtales Terrace

Andros I.

OF

⑦ (27)

STRAITS

CAY SAL No.I
TD 5762

Cay Sal Bank

SANTAREN CHANNEL

(20)

⑧ (26)

(13)

⑥

NICHOLAS CHANNEL

(24)
(23)

③ (5)

(19) ④

(21) (1)

(12)

② (17)

(22)

(6A)

(14)(5)
(16)

CAYO COCO 2
TD 3219

(15)

(6B)

(6B)

MANUY I
TD 2712

BLANQUIZAL No.I
TD 3419

C U B A

CAYO FRAGOSO
TD 5012

CAYO FRANCES
TD 4536 ?

PUNTA ALEGRE I ,TD657

COLLAZO I, TD 4260

PUNTA ALEGRE 2
TD 1416

TINA I
TD 3420

26°

25°

24°

23°

22°

82°   81°   80°   79°   78°

Figure 1.

A

CAYO FRAGOSA
TD 5012

CAYO FRANCES
TD 4536?

A'

CAIBARIÉN

LAS VILLAS PROV.

U PUNTA ALEGRE FAULT
D

S. DE JATIBONICO

PLACETAS

X-SECTION FIG 2B

JARAHUECA FENSTER

A

SIERRA DE TRINIDAD

LA TROCHA FAULT ZONE

COLLAZO I TD 4260

PUNTA ALEGRE DIAPIR

PUNTA ALEGRA I TD 657

B ZONE

MANUY I TD 2712

PUNTA ALEGRA 2 TD 1416

B'

CAYO COCO 2 TD 3219

ATLANTIC OCEAN

CAYO COCO

ISLA TURIGUANÓ DIAPIR

MORÓN

LOMA CUNAGUA DIAPIR

MORÓN BASIN

CIEGO DE ÁVILA

CAMAGÜEY PROVINCE

SIERRA DE CUBITAS

CAYO ROMANO

C.W. HATTEN ET AL (1958)

CARIBBEAN SEA

CAMÁJAN FENSTER

0   10   20
KM

22°30'

22°00'

79°30'   79°00°   78°30'   78°00'

B

SSW

A

MANICARAGUA BATHOLITH

TRINIDAD ZONE

TRINIDAD MTS

FOMENTO

SANTA CLARA ZONE

'PLACETAS' ZONE

PLACETAS

CAMAJUANÍ ZONE

REMEDIOS ZONE

REMEDIOS

NORTH COAST

A'

NNE

UPPER JURASSIC - SENONIAN (MIOGEOSYNCLINAL FACIES)

PALEOCENE - MIDDLE EOCENE

UPPER EOCENE - MIOCENE

UPPER JURASSIC - PALEOCENE (PLATFORM FACIES)

SENONIAN - MAESTRICHTIAN (UPPER CRETACEOUS, S. CUBA)

APTIAN - SENONIAN EUGEOSYNCLINAL FACIES

SENONIAN GRANITIC ROCKS

UPPER JURASSIC (?) - NEOCOMIAN SERPENTINITE AND GABBRO COMPLEX

AMPHIBOLITES (VARIOUS AGES?)

JURASSIC, PUNTA ALEGRE FORMATION

METAMORPHIC ROCKS, PRE - UPPER JURASSIC

ACIDIC - BASIC CRYSTALLINE BASEMENT ROCKS

0   5   10   15   20
KILOMETERS

MODIFIED FROM DUCLOZ AND VUAGNAT (1962), WASSALL (1957)

Figure 2

A

BAHÍA BUENA VISTA

PUNTA ALEGRE FAULT ZONE

B

PUNTA ALEGRE 911' I
1-A
2,156'

PUNTA
SAN JUAN

PUNTA
ALEGRE

PUNTA ALEGRE
SUGAR MILL

PUNTA ALEGRE
DIAPIR

CAYO
LADRONES

COLLAZO 13,019'
I

LAS VILLAS PROVINCE

Río Jaribonico Del Norte

CAMAGÜEY PROVINCE

22°20'N

Río Los Perros

ISLA TURIGUANÓ

LEGEND

QUATERNARY — UNNAMED SURFICIAL DEPOSITS

MIOCENE — GÜINES LIMESTONE

OLIGOCENE — UNNAMED

JURASSIC — PUNTA ALEGRE FORMATION

A. A. MEYERHOFF

TO CHAMBAS

B'

PUNTA ALEGRE 2
4,646'

0 1 2 3 4 5
KILOMETERS

LAGUNA DE LECHE

78°50'W

B

N   S

MORÓN BASIN

PUNTA ALEGRE NO.1-A

PUNTA ALEGRE FAULT

SHORE LINE

PUNTA ALEGRE HILLS

COLLAZO NO.1

PUNTA ALEGRE NO.2

BAHÍA BUENA VISTA

B   B'

MIOCENE

S.L.

U. EOCENE - OLIGOCENE

L.&M. EO.

L.&M. EOCENE

OLIGOCENE

MIOCENE

OLIGOCENE

LATE MIDDLE AND UPPER EOCENE

T.D 2,156 (653 m)

SALT

LOWER AND MIDDLE AND MAESTRICHTIAN EOCENE

LOWER AND MIDDLE EOCENE

T.D 4,646' (1,408 m)

T.D 13,019' (3,945 m)

LEGEND

LATE MIDDLE EOCENE - MIOCENE

LOWER AND MIDDLE EOCENE, MAESTRICHTIAN

ALBIAN - SENONIAN

PORTLANDIAN - ALBIAN

JURASSIC, PUNTA ALEGRE FORMATION

A.A MEYERHOFF

0 1000 2000 3000

VERTICAL AND HORIZONTAL SCALE IN METERS

Figure 3

Figure 4

LEGEND

Sandstone	Limestone	Anhydrite	Volcanics of basic composition
Siltstone	Dolomite	Salt	Tuff
Shale		Volcanics of mixed composition	Discordance
Clay			
Marl			

Figure 5

47

A

10 KM

N   S

V.E. ≅ 11/1

NW   B   SE | WNW   ESE

10 KM

V.E. ≅ 15/1

Figure 6

```
┌─────────────┐
│ Demultiplex │
│ field tapes │
└─────────────┘
        │
        ├──────────────────────►  ╭─────────────╮
        │                         │ Display     │
        ▼                         │ shot records│
┌──────────────────┐             ╰─────────────╯
│ Geometry         │
│ Horizontal scale │
│ CDP sort         │
└──────────────────┘
        │              ┌──────────────────┐      ┌──────────────────┐
        ├─────────────►│ Edit 5 CDPs      │◄────►│ Filter analysis  │
        │              │ every 50 CDPs    │      │        &         │
        │              │ for velocity     │      │ DCON analysis    │
        │              │ analysis         │      └──────────────────┘
        ▼              └──────────────────┘
┌──────────────────┐            │
│ Spherical        │            ▼
│   divergence     │  ┌──────────────────┐
│ Bandpass filter  │  │ Bandpass filter  │
│ Predictive DCON  │  │ Predictive DCON  │
│ Mute             │  │ Mute             │
│ NMO correction   │  │ AGC scale        │
│ Stack            │  │ Velocity analysis│
└──────────────────┘  └──────────────────┘
        │                      │        ╭──────────╮
        │                      ├───────►│ Display  │
        ▼                      │        │ velocity │
   ╭─────────╮                 │        │ analysis │
   │ Raw     │                 ▼        ╰──────────╯
   │ stack   │        ┌──────────────────┐   ╭─────────────────╮
   │ tape    │        │ Apply velocity   ├──►│ Display NMO corr.│
   ╰─────────╯        │ functions for    │   │ CDP gathers     │
        │             │ quality control  │   ╰─────────────────╯
        │             └──────────────────┘
        ├─────────────► ┌──────────────────┐
        │               │ Filter analysis  │
        │               │        &         │
        │               │ DCON analysis    │
        ▼               └──────────────────┘
┌──────────────────┐    ╭──────────╮
│ Time - variant   │    │ True     │      ╭──────────╮
│ bandpass filter  ├───►│ relative │─────►│ Section  │
│                  │    │ amplitude│      │ to film  │
│ Long period      │    │ stack    │      ╰──────────╯
│ predictive DCON  │    │ tape     │
└──────────────────┘    ╰──────────╯
        │
        ▼
┌──────────────────┐
│ Short window     │
│ AGC scale        │
└──────────────────┘
        │
        ▼
   ╭─────────╮       ╭──────────╮
   │ Scaled  │       │ Section  │
   │ stack   ├──────►│ to film  │
   │ tape    │       ╰──────────╯
   ╰─────────╯
```

Figure 7

Figure 8

Unsmoothed iso-velocity plot

Two-way time, seconds

Figure 9

Smoothed iso-velocity plot
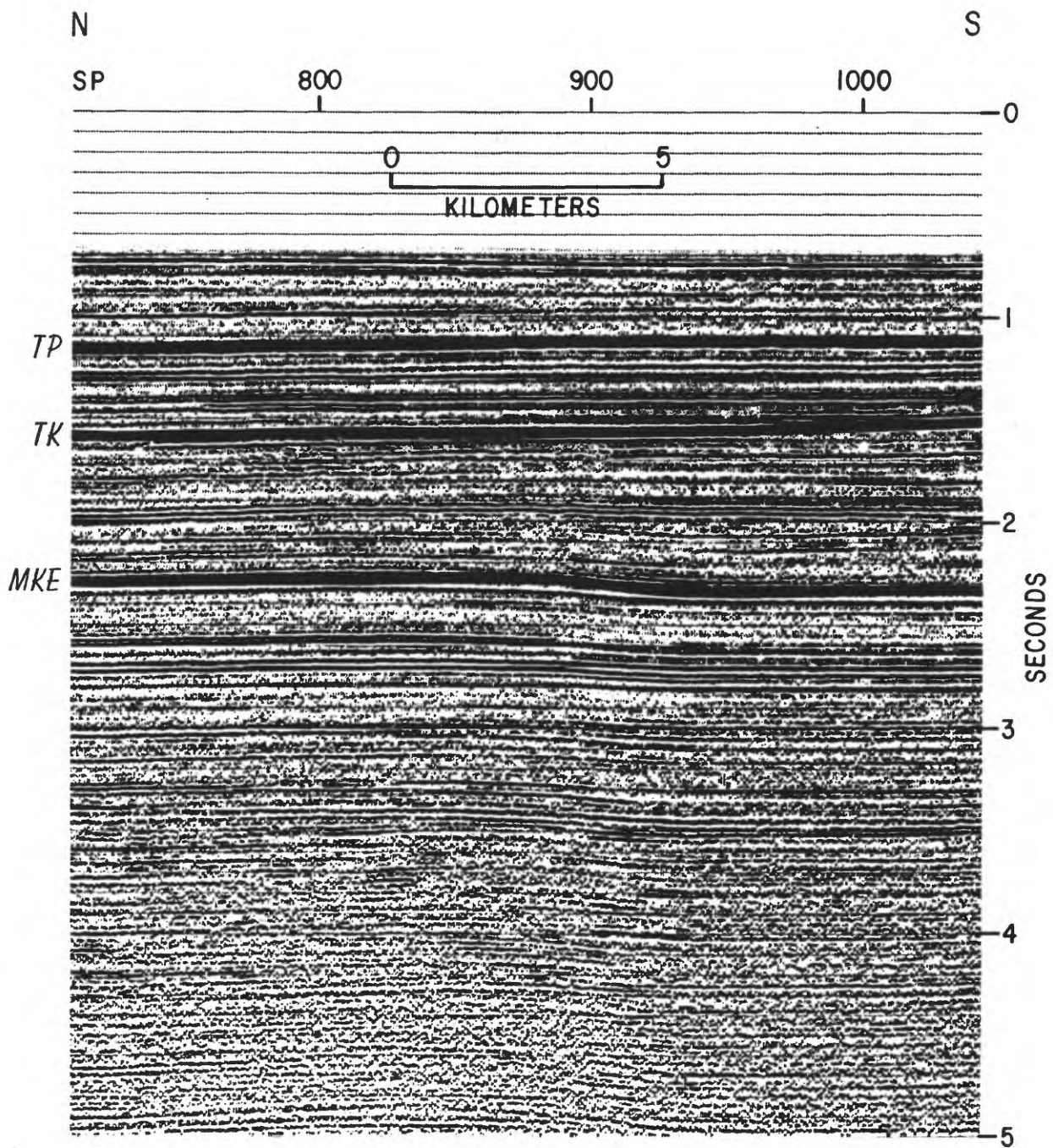
Two-way time, seconds
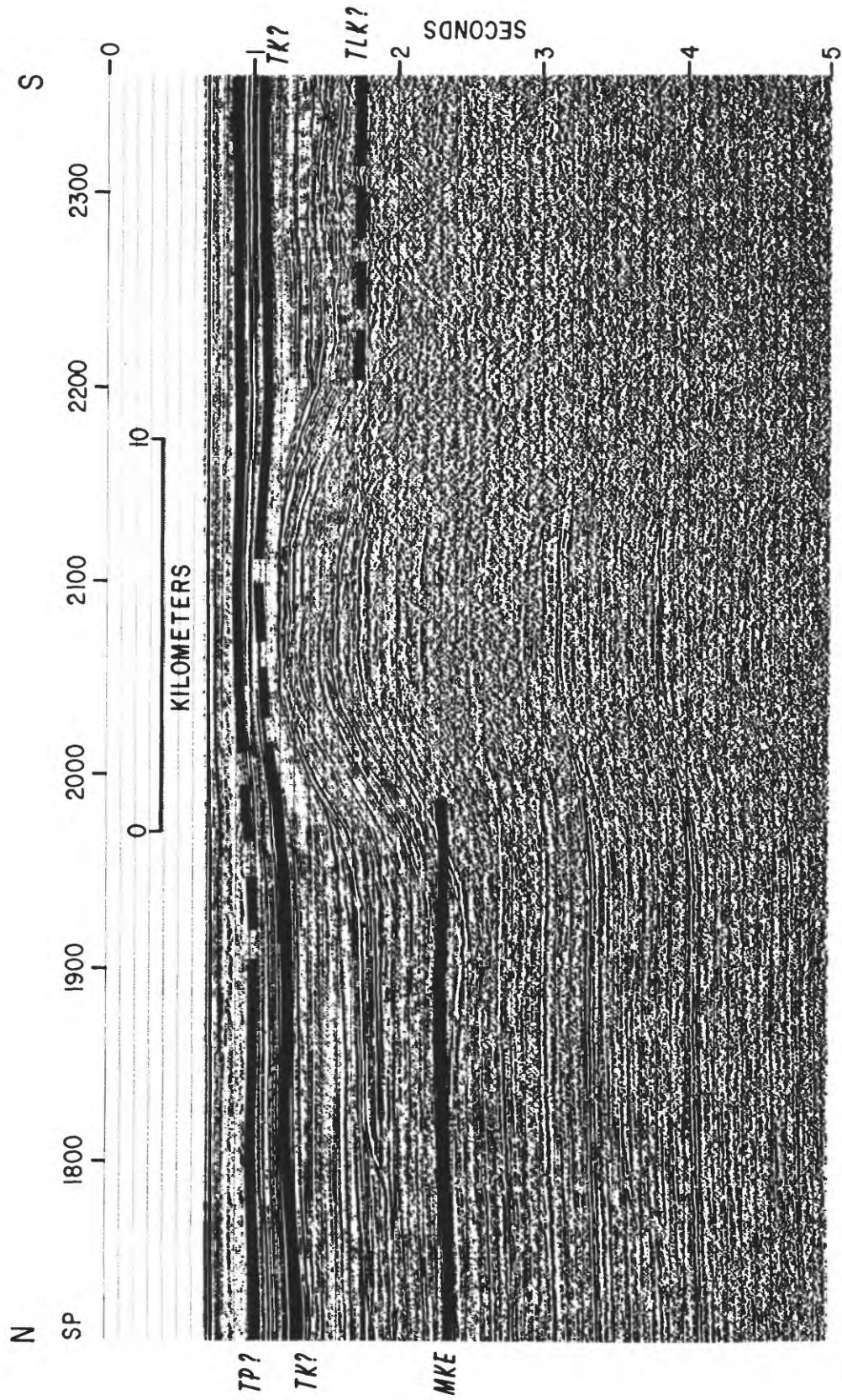
Figure 10

Figure 11

Figure 12

54

Figure 13

Figure 14
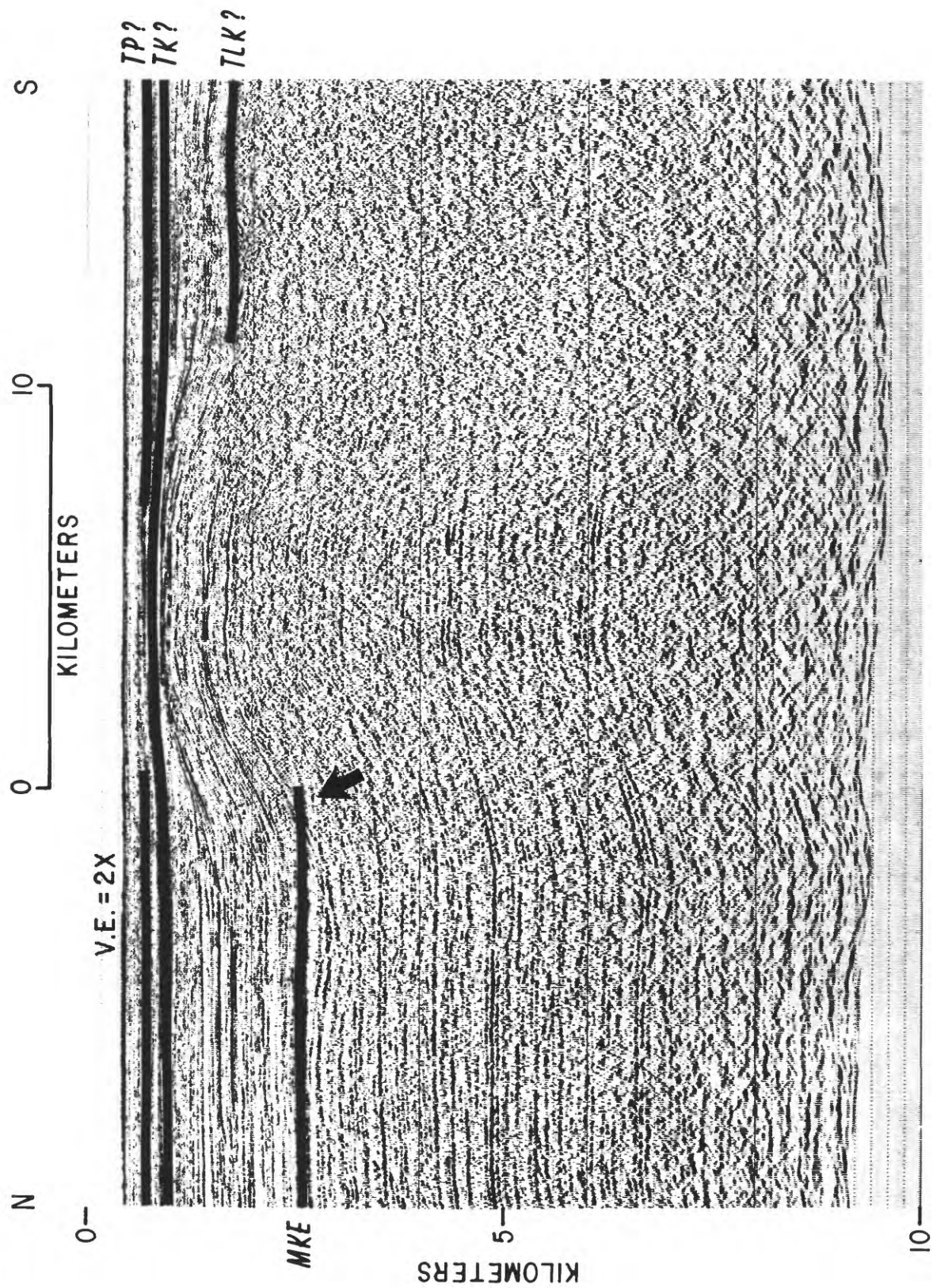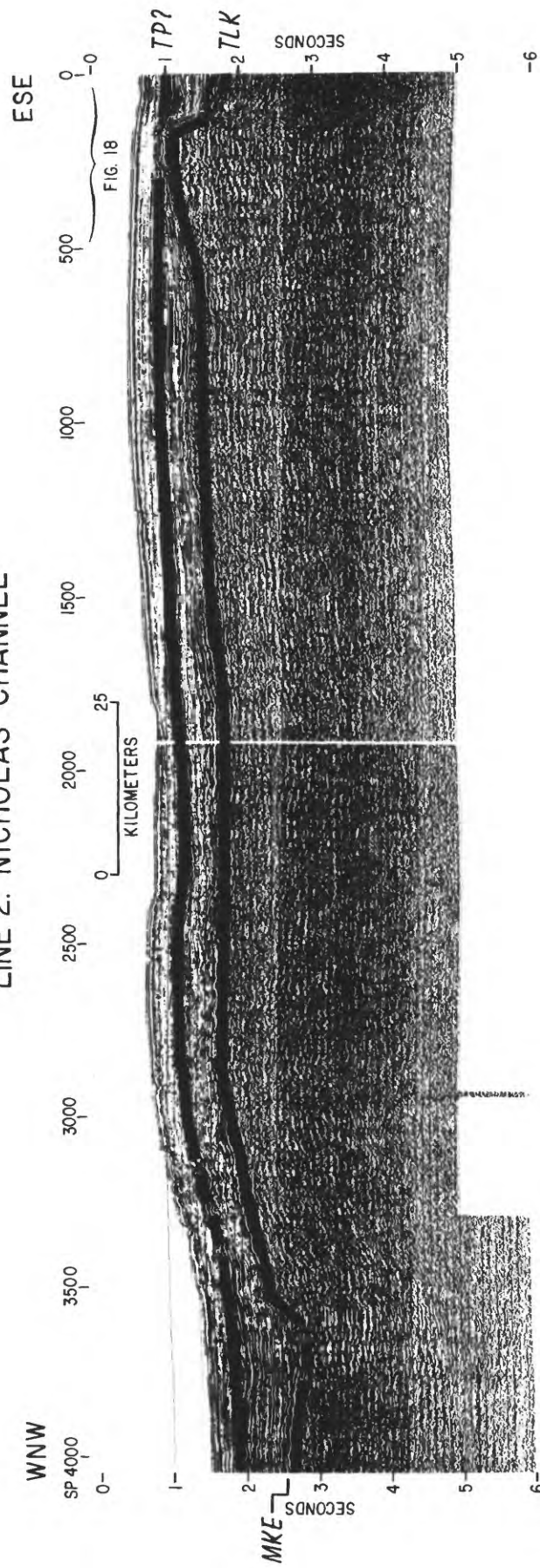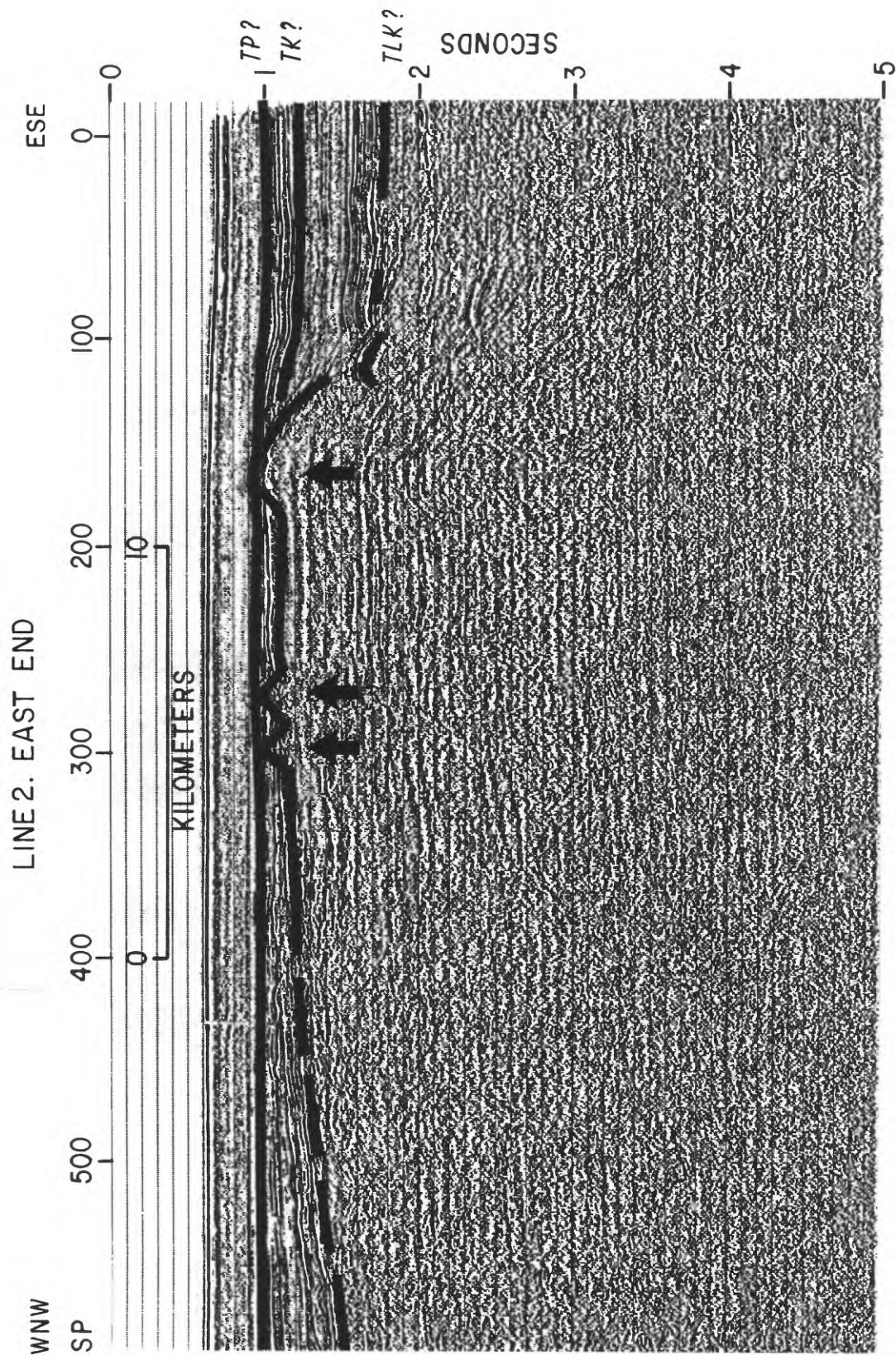
Figure 15

Figure 16

LINE 2. NICHOLAS CHANNEL

Figure 17

LINE 2. EAST END
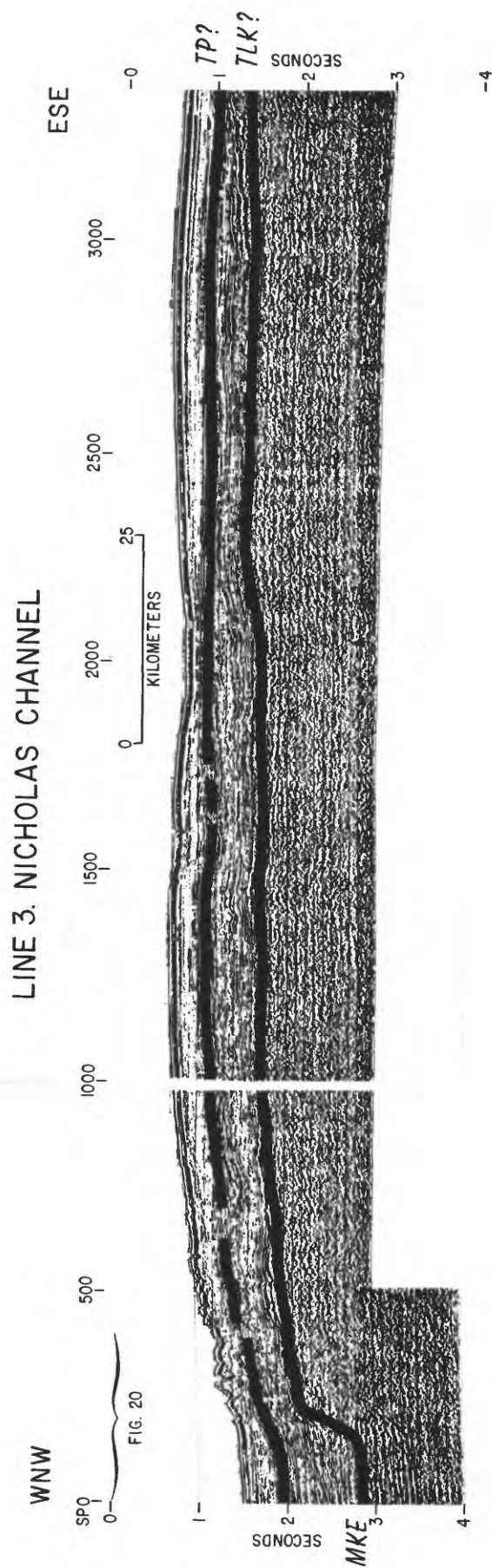
Figure 18

60

LINE 3. NICHOLAS CHANNEL

Figure 19

LINE 3. WEST END

Figure 20

62

Figure 21

63

Figure 22

LINE 4. EAST END

SECONDS

SE

NW

SP 300

KILOMETERS

TP?

TK

64

Figure 23

65

LINE 5. SANTAREN CHANNEL
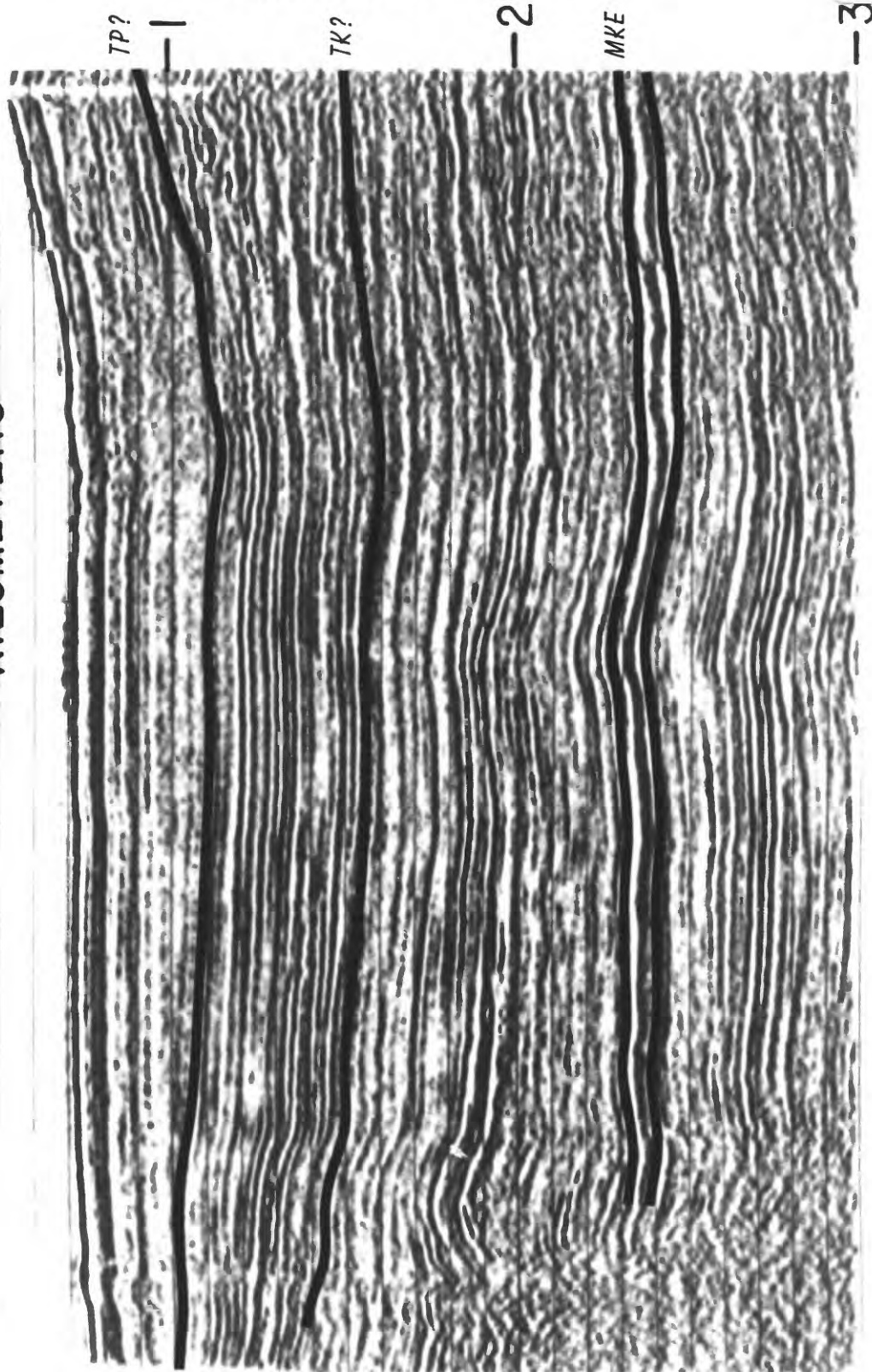
Figure 24

Figure 25
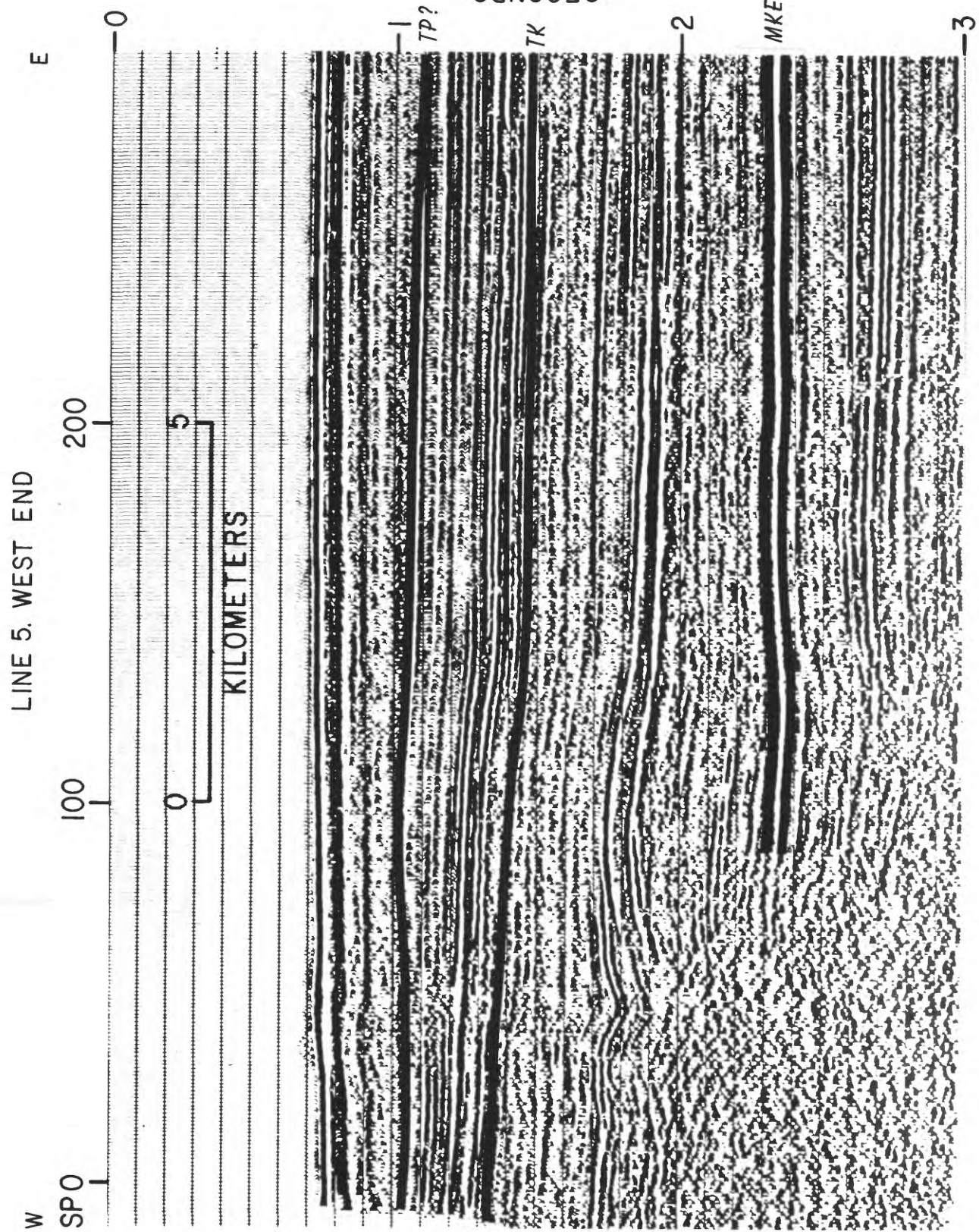
LINE 6. SANTAREN CHANNEL
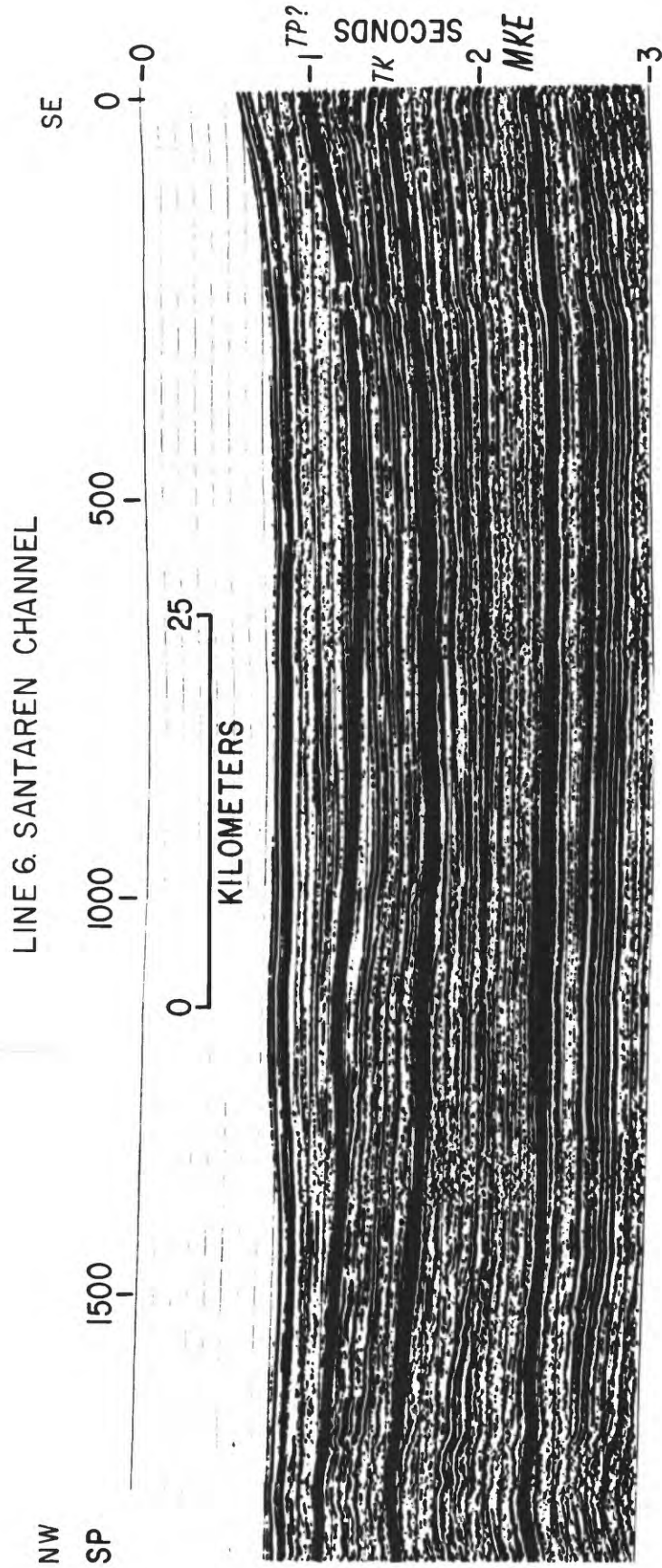
Figure 26

LINE 7. SANTAREN CHANNEL

Figure 27

69

Figure 28

STRUCTURAL DIAGRAM OF CUBA

Figure 29

FLORIDA—BAHAMA PLATFORM

LARAMIDE RHEOGENETIC COMPLEX

MILD LARAMIDE FOLDS

LARAMIDE TRANSPORTED MATERIAL

GRANITE & METAMORPHIC MASSES

DIRECTION OF TRANSPORT

DIRECTION OF GLIDING

GULF OF MEXICO

OLD BAHAMA CHANNEL

CARIBBEAN SEA

BARTLETT DEEP

0   100   200

KM

71

Figure 30